ACS APPLIED MATERIALS & INTERFACES

Research Article

www.acsami.org

Enhanced Electrochemical Performance of Hydrous RuO_2/Mesoporous Carbon Nanocomposites via Nitrogen Doping

Chuanfang Zhang,[†] Yingbo Xie,[§] Mengqiang Zhao,[‡] Amanda E. Pentecost,[‡] Zheng Ling,[‡] Jitong Wang,[†] Donghui Long,*[,†] Licheng Ling,[†] and Wenming Qiao*[,†]

[†]State Key Laboratory of Chemical Engineering, East China University of Science and Technology, Shanghai 200237, China

[‡]A.J. Drexel Nanomaterials Institute, Department of Materials Science and Engineering, Drexel University, Philadelphia, Pennsylvania 19104, United States

[§]Titan Chem Co., LTD, Shanghai 200237, China

Supporting Information

ABSTRACT: Hydrous RuO_2 nanoparticles have been uniformly deposited onto nitrogen-enriched mesoporous carbons (NMCs) via a facile hydrothermal method. The nitrogen doping in the carbon framework not only provides reversible pseudocapacitance but also guides uniform deposition of RuO_2 nanoparticles. As a result, an extremely high specific capacitance of 1733 F/g per RuO_2, comparable to the theoretic capacitance of RuO_2, is reached when 4.3 wt % of $RuO_2 \cdot 1.25H_2O$ is loaded onto the NMCs. Systematic studies show that either nitrogen-free or excess nitrogen doping result in RuO_2 clusters formation and worsen the electrochemical performances. With intermediate nitrogen and RuO_2 content (8.1 wt % N, 29.6 wt % of $RuO_2 \cdot 1.25H_2O$), the composites deliver excellent power performance and high specific capacitance (402 F/g) with reversible capacitive response at 500 mV/s. The unique properties of nitrogen in textual, morphological, and electrochemical aspects may also provide further understanding about the effects of nitrogen doping and metal oxide deposition on supercapacitor performance.

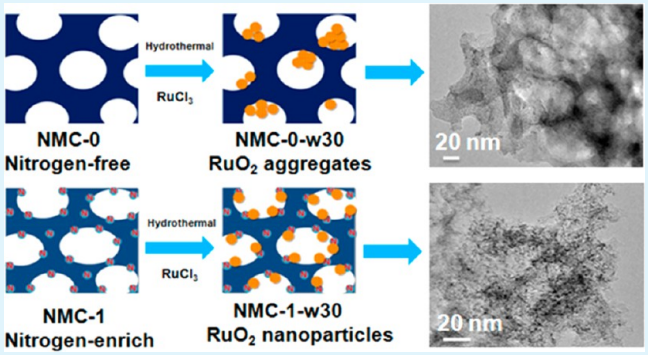

KEYWORDS: *pseudocapacitor, ruthenium oxide, nitrogen-enriched mesoporous carbon, high power performance, hydrothermal method*

1. INTRODUCTION

Because of their rapid charge−discharge ability and long cycle life, supercapacitors have been hailed as extremely promising energy storage devices to meet future energy demands.[1,2] Supercapacitors are separated into two categories: electrical double layer capacitors (EDLCs) and pseudocapacitors,[1] each based on its charge storage mechanism. EDLCs electrostatically store charge using reversible adsorption of electrolyte ions onto materials with highly accessible surface areas, while pseudocapacitors take advantage of reversible redox reactions at the surface of the electrode−electrolyte interface. Continued scientific endeavors have been directed toward designing and engineering porous carbon materials for supercapacitors because of their low cost, high surface area, and numerous geometries.[2,3] The physical ion adsorption/desorption on high-surface-area carbon materials endows supercapacitors with much higher energy densities than dielectric capacitors, although it is still significantly lower than Li ion batteries.[4]

One such way to improve the energy density of supercapacitors is by incorporating pseudocapacitance into EDLCs. Metal oxides, such as RuO_2,[5−7] MnO_2,[8] NiO,[9] and Co_3O_4,[10] are able to store more charge through highly reversible surface redox reactions. Among these oxides, RuO_2 has been intensively studied because of its wide potential window, reversible redox reaction, high theoretical specific capacitance, and high electrical conductivity (3×10^2 S/cm).[11] However, RuO_2 nanoparticles (NPs) generally suffer from severe particle aggregation, which leads to poor cycling ability and deteriorated rate performance. To circumvent these problems, many researchers have attempted to combine hydrous RuO_2 NPs with carbon materials, including activated carbons,[12] carbon nanotubes (CNTs),[13−16] carbon nanofibers,[17,18] graphene,[19,20] mesoporous carbon (MC),[21] carbon spheres,[22] carbon quantum dots,[23] and so forth. Such a hybrid material could substantially improve the utilization and rate capability of hydrous RuO_2. MCs are the most ideal substrates for hydrous RuO_2 NPs due to their excellent textural characteristics and mesoporous networks, which provide a three-dimensional interconnected framework and facilitate ion diffusion without pore blockage.[24]

Various methods such as sol−gel,[21] colloidal,[25] and impregnation methods[26,27] have been developed for the

Received: April 10, 2014
Accepted: May 21, 2014
Published: May 21, 2014

   dx.doi.org/10.1021/am502173x | ACS Appl. Mater. Interfaces 2014, 6, 9751−9759

construction of RuO_2/MC composites. For instance, Jang et al.[26] prepared their material by impregnating MCs with ruthenium(III) acetyl acetonate. The composites exhibited a capacitance of 243 F/g (per electrode) and 738 F/g (per RuO_2) at a low loading of RuO_2 (14.6 wt %). However, the specific capacitance gradually decreased to 363 F/g due to particle aggregation as the RuO_2 content was increased to 54 wt %. On the other hand, Li et al. impregnated ordered MCs in $RuCl_3$ solution followed by annealing in N_2 from 80 to 400 °C.[27] The highest capacitance per electrode reached 633 F/g. However, as the RuO_2 content was increased from 10.0 to 30.7 wt %, its pseudocapacitance and rate performance decreased sharply due to the increase in equivalent series resistance. Although RuO_2/MC composites represent a novel method to improve the capacitive behavior of RuO_2 itself, it is necessary to achieve not only higher specific capacitance but also per electrode as a whole. To reach this goal, a method for the homogeneous deposition of RuO_2 NPs without blocking the developed pore channels of the carbon substrate must be developed.

Previous studies demonstrated that doping with nitrogen atoms improves the hydrophilic properties of carbon frameworks and provides faradic pseudocapacitance.[28] In addition, nitrogen atoms can directly incorporate themselves into the carbon sp^2 backbone and alter the electron-donor properties of the carbon substrate.[29,30] Moreover, those nitrogen species could promote interactions between the NPs and carbon surfaces and consequently improve their dispersion. Sun et al.[31] revealed that Pt NPs distributed uniformly when the nitrogen-doped CNT-covered Si wafer is used, demonstrating that nitrogen atoms were helpful in the NP dispersion. In another instance, Fang et al. dispersed RuO_2 NPs on nitrogen-doped CNTs. The introduction of nitrogen was beneficial in the creation of preferable sites for the uniform distribution of NPs, leading to a significant improvement in the overall capacitance.[32,33] However, reports on the preparation of nitrogen-doped MC composite electrodes with high metal oxide loadings are quite limited.

In order to address previous shortcomings, a novel material design should exploit a combination of the hydrophilic properties of doped nitrogen, the high pseudocapacitance of metal oxides and the nitrogen species, and the desirable power behavior of MCs. Therefore, in this study, the nitrogen-enriched mesoporous carbons (NMCs)[28] were used as substrates to host hydrous RuO_2 NPs. Through tuning the weight ratio of the $RuCl_3$ to NMCs, a series of composites with varied RuO_2 content were prepared with a maximum loading of 68.9 wt %. Furthermore, in order to systematically study the dual effect of nitrogen species and RuO_2 loading on the physical and electrochemical properties of composites, nitrogen content-series with the same RuO_2 loading were also prepared. The promising capacitive performances suggest the synergetic effect of the RuO_2 nanoparticles and nitrogen species. In addition to pseudocapacitor applications, this composite material could also be used as a gas catalyst and an electrode for fuel cells.

2. EXPERIMENTAL SECTION

2.1. Preparation of NMCs. NMCs were synthesized according to our previous report.[28] Typically, 39 mmol of phenol (P) and 78 mmol of formaldehyde (F, 37 wt %) were dissolved in 10 mmol of NaOH solution and stirred at 70 °C for 40 min. Then, 39 mmol of melamine (M) and 107 mmol of formaldehyde were added to the above solution and stirred at 80 °C for 30 min until the solution become clear. Next, 50 g of Ludox SM-30 sol (30 wt % SiO_2) was added to the above solution and stirred at 80 °C for an additional 5 min. The concentration of colloidal silica in the polymer mixture (M + P + F) was fixed at 15 g/100 mL. The concentration was fixed at 18 g/10 mL for the nitrogen-free samples. Finally, the obtained gels were sealed into ampules and placed in the oven at 80 °C for 3 days, followed by carbonization in nitrogen at 800 °C for 3 h. After dissolution of the silica nanoparticles in 2 M NaOH solution at 80 °C for 12 h, NMCs were filtrated, washed with DI water until the pH was approximately neutral, and then, purged under vacuum at 90 °C overnight. The obtained samples were denoted as NMC-*x*, where *x* represents the mole ratio of melamine to phenol.

2.2. Preparation of NMC/RuO_2 Nanocomposites. The NMC/RuO_2 composites were prepared through a facile hydrothermal method. Specifically, 70 mg of NMC-1 powder was sonicated in 60 mL of DI water for 10 min. Then, 4.664 g of ruthenium chloride of 1 wt % (in DI water) was added drop-by-drop into the above suspension, and the mixture was sonicated for another 10 min. The suspension was transferred to a Teflon-lined autoclave with a stainless-steel shell and kept at 180 °C for 6 h. After cooling down naturally, the product was filtered, washed with DI water, and centrifuged until the pH reached 7. The composites were dried at 80 °C for 24 h and denoted as NMC-1-w30, indicating that the theoretical weight percentage of ruthenium oxide in the composite was 30 wt %. Composites with different nitrogen content were prepared with RuO_2 loading of 30 wt % using NMC-*x* as a substrate and were denoted as NMC-*x*-w30. Also, composites with different RuO_2 loading were prepared using NMC-1 and were denoted as NMC-1-wy. For example, NMC-1-w10 and NMC-1-w70 represent mass loadings of RuO_2 of 10 and 70 wt %, respectively.

2.3. General Characterizations of the Materials. The X-ray diffraction (XRD) patterns were acquired on a Rigaku D/max 2550 diffractometer operating at 40 kV using Cu Kα radiation (λ = 1.5406 Å). Nitrogen adsorption/desorption isotherms were conducted at 77 K on a Quadrasorb SI analyzer. Before the measurements, the samples were degassed in vacuum at 373 K for 6 h. The Brunauer–Emmett–Teller (BET) method was utilized to calculate the specific surface area. Pore size distributions (PSDs) were derived from the desorption branch by using the Barrett–Joyner–Halenda (BJH) model. Elemental analysis was carried out on an Elemental Vario EL. The carbon (C), hydrogen (H), and nitrogen (N) contents were determined directly using a thermal conductivity detector. The surface composition of the NMCs was obtained from an Axis Ultra DLD X-ray photoelectron spectrometer. Thermogravimetric analysis (TGA) was performed on a Q50 TGA Analyzer (TA Instruments) using a temperature range from room temperature to 800 °C at 5 °C/min. Scanning electron microscopy (SEM) images of the pristine NMC-1 and nitrogen-RuO_2 composites were obtained on Zeiss Supra 50VP (Carl Zeiss AG, Germany). Transmission electron microscopy (TEM) was conducted on a JEM 2100 (JEOL, Japan) using an accelerating voltage of 200 kV. The samples were first dispersed in isopropanol and then sonicated for 1 min. A drop of this mixture was transferred onto a 200 mesh lacey-carbon-coated copper grid for imaging.

2.4. Preparation of Electrodes and Electrochemical Setup. Both the active material and carbon black were dispersed in 1-methyl-2-pyrrolidone (NMP) to form a suspension with a concentration of 20 mg/mL. The mass ratio of active material to carbon black and nafion (binder) was 8:1:1. After vigorous stirring for 4 h, 10 μL of the slurry was cast onto the mirrorlike glassy carbon electrode (GCE) using a micropipet. The mass of the electrode was approximately 0.2 mg. The modified GCE was dried at 60 °C for 1.5 h and soaked for 1 h prior to the tests.

All the electrochemical tests were conducted in a sealed three-electrode cell with 1 M H_2SO_4 (0–1 V) as the electrolyte, the modified GCE as the working electrode, and platinum wire and Ag/AgCl as the counter and reference electrodes, respectively. Cyclic voltammetry (CV) (PCI-4/300 potentiostat, Gamry, PA, USA) and galvanostatic charge–discharge (GCD) (Arbin instrument, TN, USA) were conducted with scan rates and current densities ranging from 10

Table 1. Pore Parameters and RuO_2 Contents of NMCs and Their Composites

sample	S_{BET} [a] (m^2/g)	V_{total} [b] (cm^3/g)	V_{meso} (cm^3/g)	D_{av} [c] (nm)	N[d] (wt %)	ash (wt %)	$RuO_2 \cdot xH_2O$[e] (wt %)
NMC-0	696	2.40	2.25	12.6	0	0.2	–
NMC-0.5	777	2.30	2.16	13.2	4.3	0.2	–
NMC-1	731	2.60	2.49	13.8	8.1	0.2	–
NMC-2	771	2.40	2.31	11.6	11.9	0.3	–
NMC-1-w10	560	2.23	2.16	14.8	8.1	3.7	4.3
NMC-1-w30	467	1.59	1.56	14.5	8.1	25.5	29.6
NMC-1-w70	301	0.48	0.46	10.4	8.1	59.4	68.9
NMC-0-w30	344	1.21	1.19	14.0	0	24.8	29.0
NMC-0.5-w30	376	1.34	1.33	14.3	4.3	25.1	29.3
NMC-2-w30	368	1.12	1.11	12.2	11.9	24.7	28.9

[a]BET specific surface area. [b]Total pore volume (P/P_0= 0.985). [c]BJH average pore width. [d]*N* wt % was the mass ratio in the carbon substrate. [e]$RuO_2 \cdot xH_2O$% was calculated proportional to RuO_2 % with x = 1.25.

to 500 mV/s and from 0.2 to 8 A/g, respectively. Specific capacitance was calculated from the GCD according to eq 1:

$$C_{spe} = \frac{i}{m \times \frac{\Delta V}{\Delta t}} = \frac{j}{\frac{\Delta V}{\Delta t}} \quad (1)$$

where C_{spe} (F/g) is the specific capacitance of the active material, m is the active mass, j is the current density (A/g) applied on the working electrode, t is the discharge time (s), and V is the potential window (V) after the IR drop.

3. RESULTS AND DISCUSSION

3.1. NMC/RuO_2 Composites. Systematic studies have been done in our previous report about the effect of nitrogen doping on the porosity, conductivity, and electrochemical performances of NMCs.[28] Typically, we have managed to prepare the nitrogen-enriched carbon with very similar mesoporous structures but different nitrogen content in the range 0−11.9 wt %. This could thus minimize the influence of the porosity while focusing on nitrogen doping on the properties of the resulting composites. The porosity parameters and chemical nature of MCs used in this work were summarized in Table 1. These samples have a similar mesoporous structure with a pore volume around 2.3 cm^3/g and an average pore size of approximately 11 nm. The fully developed mesopores and large mesoporous ion diffusion channels for the supercapacitor electrode are clearly advantageous in high power applications. Moreover, in this work, NMCs were used as carbon framework to host RuO_2 NPs with the hope that the doping of nitrogen could improve the dispersion of the easily aggregated RuO_2.

Figure 1 shows the schematic of preparation of NMC/RuO_2 composites via a facile hydrothermal method. NMC-1 and NMC-1-w30 were selected as the typical samples here to understand the structure and properties of the NMC/RuO_2 composites. The SEM image in Figure 2a suggests the typical morphology of the NMC/RuO_2 composites. The energy-dispersive X-ray spectroscopy (EDX) result in Figure S1 (Supporting Information) suggests the loading of a large amount of RuO_2 on the NMCs; no other impurity was detected. The apparent disordered carbon with highly mesoporous structure could be clearly seen in Figure 2b. Moreover, hierarchical pore distribution of NMC is also obvious as both large mesopores (~20 nm) and intermediate mesopores (~5 nm) are found. After hydrothermal deposition, the surface of NMCs is decorated by numerous tiny RuO_2 particles with their hierarchical pore structures retained (Figure 2c). The high-resolution TEM (HRTEM) image of NMC-1-w30 in Figure 2d reveals the RuO_2 particles are uniformly

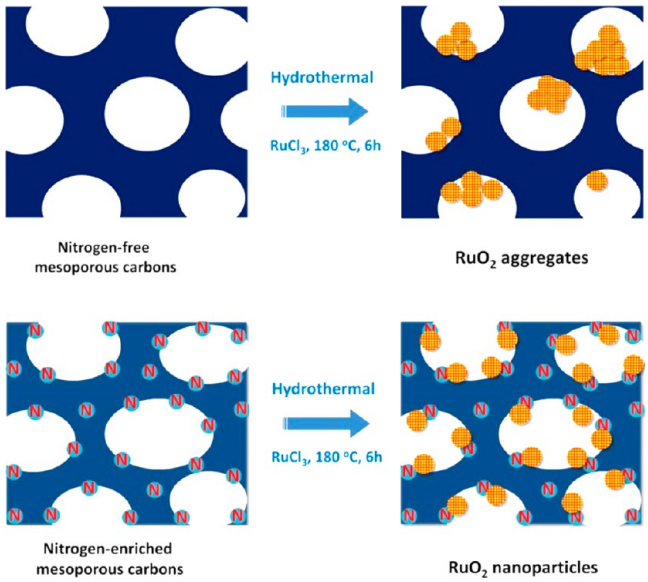

Figure 1. Schematic of preparation of NMC/RuO_2 composites.

distributed with a mean size of 2 nm. The as-prepared RuO_2 NPs are amorphous in Figure 2d. Figure 3a shows the XRD patterns of NMC-1, NMC-1-w30, and p-RuO_2. Unlike p-RuO_2 that has multiple characteristic peaks due to large RuO_2 domains, no additional peaks except for one broad diffraction peak centered at 25° in NMC-1-w30 is observed, further indicating amorphous RuO_2 has been achieved.[13−15,17,18] Broad diffraction peaks at 25° and 44° in NMC-1 correspond to reflection from the (002) and (100) planes of hexagonal graphite, respectively, (JCPDS card no. 75-1621).

The actual loading of RuO_2 in the composites could be determined through TGA, as shown in Figure 3b. Two stages of weight loss, below T_{ct} (carbon combustion temperature) and after T_{ct}, are seen in both NMC-1 and NMC-1-w30, which can be attributed to the removal of absorbed water (physically and chemically) and carbon combustion, respectively. Since the amounts of ash of the NMCs are almost the same (~0.2 wt %), as Figure S2a (Supporting Information) depicts, RuO_2 loading in the composites therefore roughly equals the reside content and is summarized in Table 1. According to Cormier et al.,[25] the hydrous number in the hydrous p-RuO_2 can be calculated from TGA total loss. By using this method, the hydrous number in the composites is determined to be 1.25. Figure S2b (Supporting Information) shows TGA of NMC-1-wy. The RuO_2 content obtained from TGA was converted into $RuO_2 \cdot$

dx.doi.org/10.1021/am502173x | ACS Appl. Mater. Interfaces 2014, 6, 9751−9759

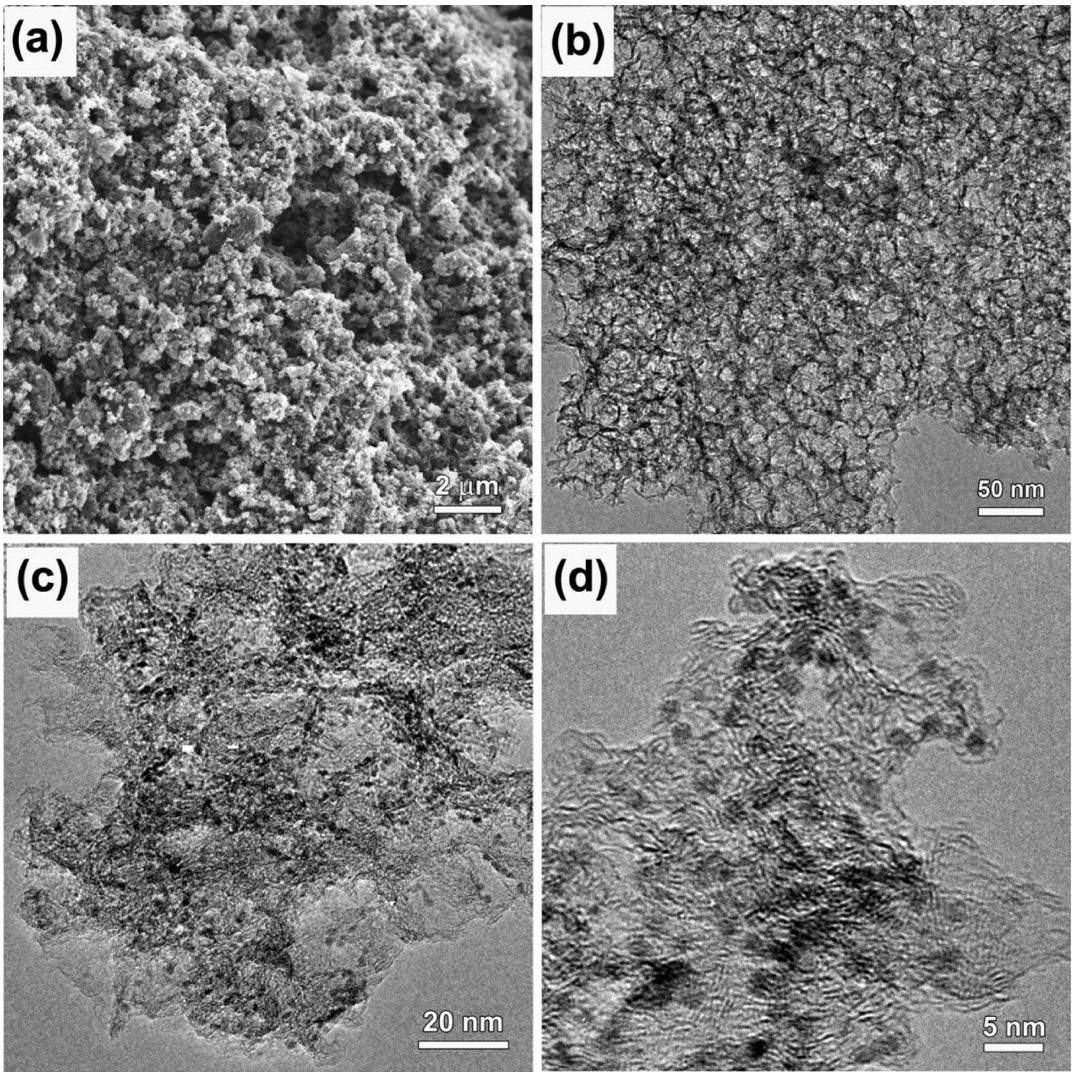

Figure 2. (a) SEM image of NMC-1-w30; TEM images of (b) NMC-1 and (c) NMC-1-w30; (d) HRTEM image of NMC-1-w30.

$1.25H_2O$ content in the composite; for example, 25.5 wt % of RuO_2 in NMC-1-w30 corresponds to 29.6 wt % of $RuO_2 \cdot 1.25H_2O$. The loading of $RuO_2 \cdot 1.25H_2O$ in the composites are quite close to the theoretical loading except in NMC-1-w10, which is probably due to the fact that the small amount loading leads to relatively larger deviation.

Figure 3c, d shows the N_2 adsorption−desorption isotherms and PSDs of NMC-1 and NMC-1-w30. NMC-1 shows a typical type-IV isotherm with an H2 hysteresis loop, corresponding to a substantial amount of mesopores. The BET specific surface area (S_{BET}) and pore volume of NMC-1 are 731 m^2/g and 2.6 cm^3/g, respectively. After depositing RuO_2, NMC-1-w30 shows expected decreases in S_{BET} (467 m^2/g) and pore volume (1.59 cm^3/g). However, the PSDs, average pore size, and the shape of the isotherms between the two samples are all similar, suggesting the composites have well inherited the pore structure.

A three-electrode system was used to evaluate the electrochemical performance of the NMC/RuO_2 composites, which are shown in Figure 4. At 200 mV/s, nitrogen species in NMC-1 still provide the pseudocapacitance, as a broad redox peak in 0−0.6 V (vs Ag/AgCl), demonstrating the doped nitrogen is competent for fast rate redox reactions (Figure 4a). NMC-1-w30 exhibits a larger CV encircled area with a symmetric CV shape, representing a higher pseudocapacitance and reversible redox reactions have taken place attributed to the loading of RuO_2 NPs. Moreover, the excellent power handling performance of NMC-1-w30 could be seen in Figure 4b, as a capacitive response can be maintained up to 500 mV/s. The symmetric GCD profiles of NMC-1-w30 in Figure 4c show a negligible IR drop at 8 A/g, suggesting a short time constant, small ESR, and reversible pseudocapacitve reactions. As a result, the specific capacitance of NMC-1-w30 reaches 401 F/g per electrode, much higher than that of NMC-1 (245 F/g) at 0.2 A/g (Figure 4d). The improved pseudocapacitance in NMC-1-w30 could be attributed to the synergistic effect between the RuO_2 NPs and the nitrogen species.

3.2. Effects of Nitrogen Content. To further optimize the electrochemical performances of the as-prepared composites, increasing the RuO_2 loading or nitrogen content to provide higher pseudocapacitance while retain a homogeneous particle distribution would be a plausible way. Therefore, NMC-*x*-w30 with different nitrogen content and NMC-1-wy with different RuO_2 loading were prepared, and their electrochemical behaviors were systematically studied. Figure 5 compares the TEM images of NMC-*x*-w30, where x = 0, 0.5, 1.0, and 2.0 corresponding to 0 wt % N, 4.3 wt % N, 8.1 wt % N and 11.9 wt % N, respectively, in the NMCs substrate. Apparently, large

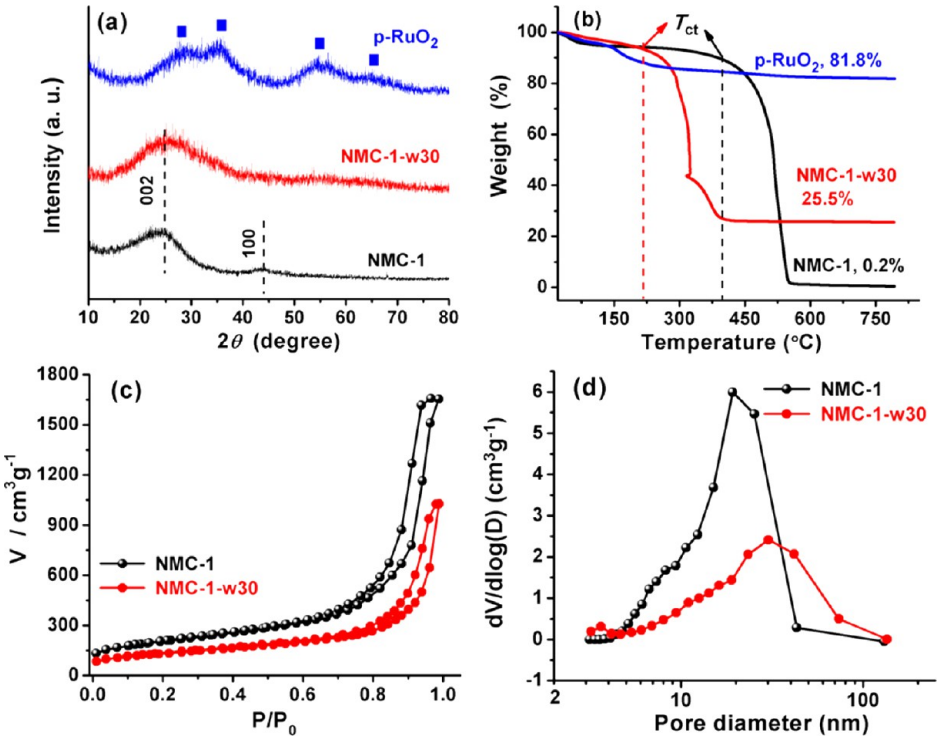

Figure 3. (a) XRD patterns of NMC-1, NMC-1-w30, and p-RuO_2; (b) TGA profiles of NMC-1, NMC-1-w30, and p-RuO_2; (c) N_2 adsorption−desorption isotherms; (d) the corresponding BJH pore size distributions of NMC-1 and NMC-1-w30.

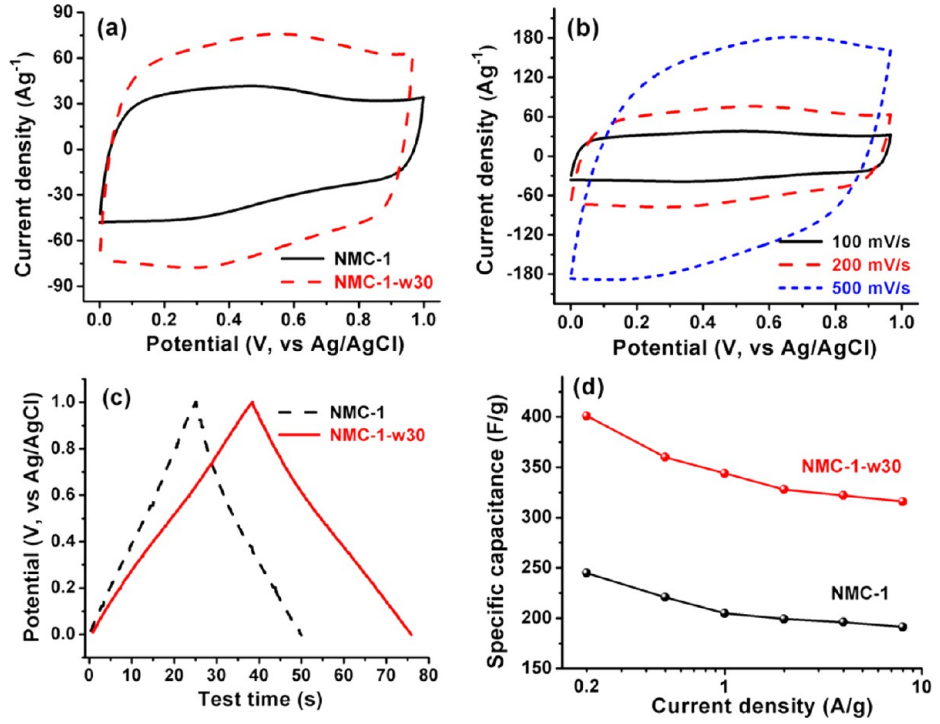

Figure 4. (a) Cyclic voltammograms of NMC-1 and NMC-1-w30 at 200 mV/s; (b) cyclic voltammograms of NMC-1-w30 at different scan rates; (c) GCD curves of NMC-1 and NMC-1-w30 at 8 A/g; (d) specific capacitance of NMC-1 and NMC-1-w30 at different current densities.

clusters of RuO_2 with a size of 20 nm can be found in the nitrogen-free composites. Those clusters exhibit nanocrystalline textual properties, as visible RuO_2 peaks at 34° and 55° were observed in their XRD patterns (Figure S3, Supporting Information). When doped with 4.3 and 8.1 wt % nitrogen, the RuO_2 particles distributed uniformly with a much decreased particle size, which could be attributed to the doped nitrogen providing basic sites and improving the interactions between the carbon substrate and guest species.[29,30] However, further increasing the nitrogen content up to 11.9 wt % again results in the formation of larger RuO_2 clusters, as shown in Figure 5d, corresponding to the RuO_2 peak at 55° in the XRD (Figure S3,

dx.doi.org/10.1021/am502173x | ACS Appl. Mater. Interfaces 2014, 6, 9751−9759

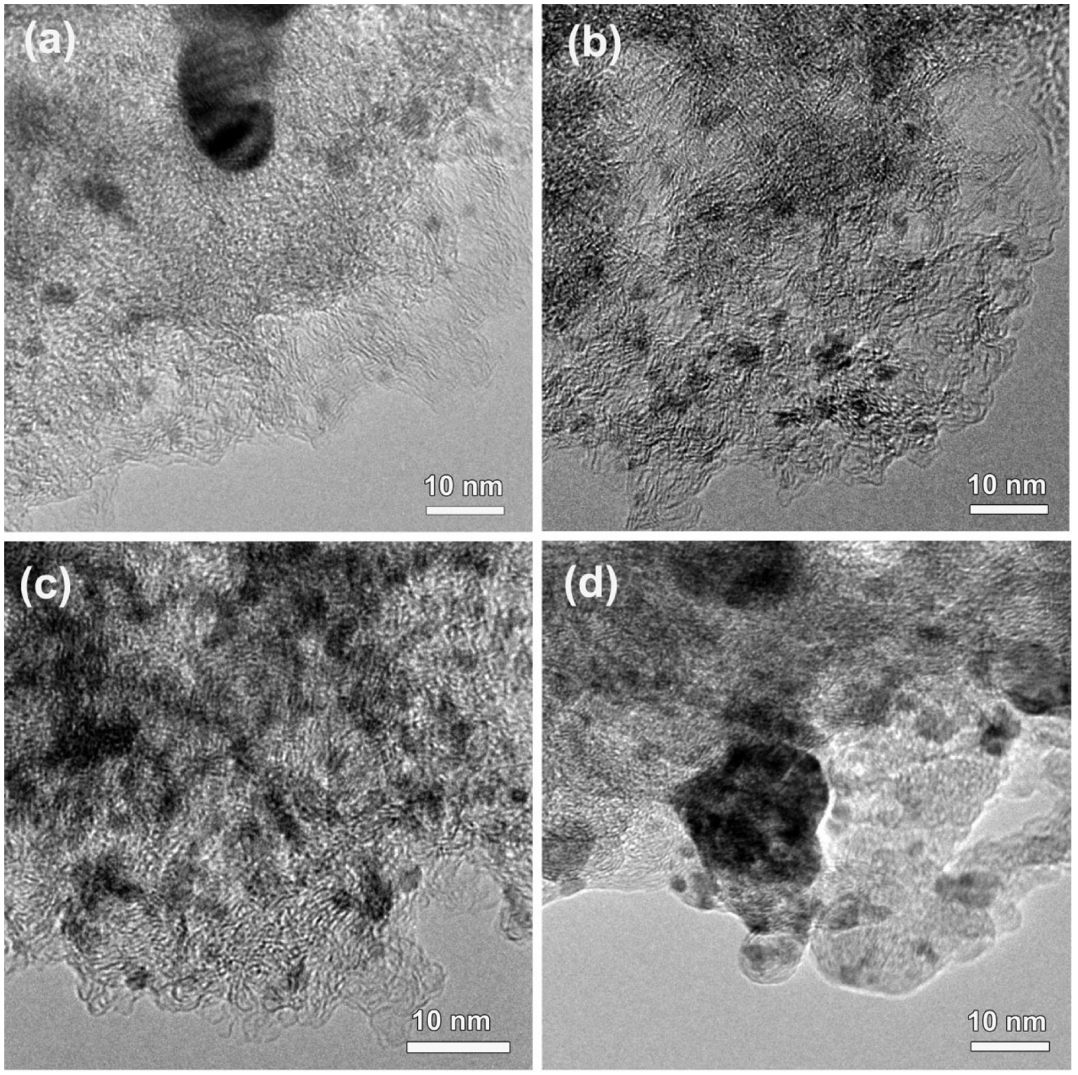

Figure 5. TEM images of (a) NMC-0-w30, (b) NMC-0.5-w30, (c) NMC-1-w30, and (d) NMC-2-w30.

Supporting Information). These TEM and XRD results provide direct experimental confirmation that nitrogen content in the composite could affect the RuO_2 dispersion to a very large extent. Doping a suitable amount of nitrogen would decrease the RuO_2 particle size and improve the distribution of the fine particles. Since the porosity parameters, including S_{BET}, pore volume, and PSDs, of NMC-*x* are similar,[28] it is not surprising to notice that NMC-*x*-w30 have similar pore volumes and S_{BET} (except for NMC-1-w30) (Table 1), which helps to avoid the complication of having different pore structures while focusing on the effect of nitrogen doping.

Figure 6 shows the electrochemical performances of NMC-*x*-w30. The quasirectangular symmetric CV shape with a broad couple of peaks and the triangular GCD profiles in Figure 6a, b represent reversible reactions in all samples. The capacitance and rate performance are strongly dependent on the nitrogen content, as shown in Figure 6c. Due to the pseudocapacitance contribution from the redox active nitrogen species, intermediate nitrogen doping improves the capacitance and rate performance and reaches the optimum in NMC-1-w30. However, when the nitrogen content is excessive, the NMC-2-w30 does not show very impressive capacitance results. This is due to RuO_2 agglomerate formation and the decreased electronic conductivity in this nitrogen excessive composite.[28] The former limits the utilization of the RuO_2 NPs while the latter greatly depresses the electron-transfer kinetics and ultimately lowers down the specific capacitance of the composite. The electrochemical impedance spectroscopy (EIS) in Figure S4 (Supporting Information) also implies that excess nitrogen content would increase the resistance. Therefore, the total electrochemical performance of the composites relies on a balance between nitrogen content and electron conductivity of the carbon substrate. The cyclic performance of NMC-1-w30 and NMC-0.5-w30, both were doped with intermediate nitrogen and have uniform RuO_2 particle dispersion, are compared in Figure 6d. After 2500 times of constant charge−discharge at 1 A/g, NMC-1-w30 still retains 91% of its initial capacitance while NMC-0.5-w30 only retains 84%. The better cycling performance in NMC-1-w30 could probably be attributed to more anchoring sites in NMC-1-w30, leading to evenly and more strongly tethered RuO_2. Such a stronger interaction between doped nitrogen species and the RuO_2 particles could facilitate more stable reversible redox reactions in NMC-1-w30, and consequently result in better life performance.

3.3. Effects of RuO_2 Loading. Besides optimizing the nitrogen content, increasing the RuO_2 loading to promote the specific capacitance is another alternative. Table 1 summarizes

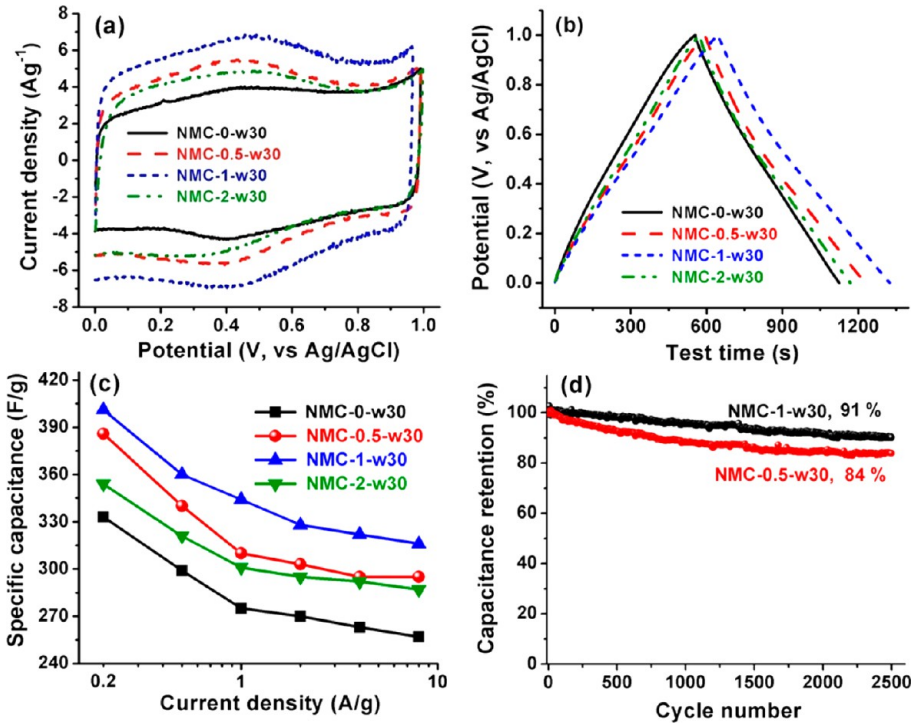

Figure 6. (a) Cyclic voltammograms at 20 mV/s; (b) GCDs at 0.5 A/g; (c) rate performance of NMC-*x*-w30; (d) cycle life performance of NMC-0.5-w30 and NMC-1-w30 after 2500 times of charge−discharge at 1 A/g.

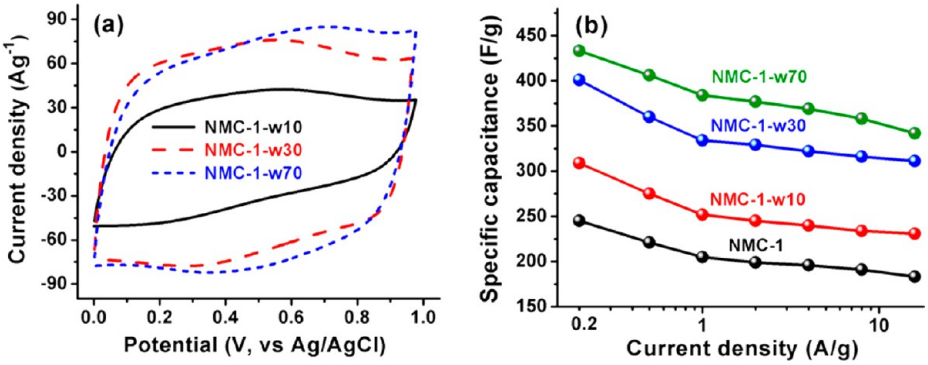

Figure 7. (a) Cyclic voltammograms of NMC-1-wy at 200 mV/s; (b) specific capacitance at various current densities.

the porosity parameters of NMC-1-wy. For example, the pore volume and S_{BET} are 0.48 cm^3/g and 301 m^2/g, respectively, in NMC-1-w70. The heavy loading not only decreased the pore volume but also formed crystalline RuO_2 with very small grains, as several characteristics peaks of crystalline RuO_2 appear in Figure S3 (Supporting Information). Previous reports suggest that amorphous RuO_2 is more desirable than the crystalline RuO_2 due to the former allowing the whole bulk of material to be used for proton diffusion and redox reactions.[11,34] Therefore, the effect of heavy loading should be carefully studied. Figure S5a (Supporting Information) and Figure 7a show the CV of NMC-1-wy at 20 and 200 mV/s, respectively. At 20 mV/s, all the CVs have a couple of broad peaks, which are indicative of pseudocapacitance from RuO_2. Close examination reveals that the cathodic peak and anodic peak in NMC-1-w70 shift positively to 0.51 and 0.55 V (vs Ag/AgCl), respectively. The CV of NMC-1-w70 is quite similar to the CV of p-RuO_2 (not shown here), due to the aggregated nanocrystalline RuO_2 in both samples. Increasing the RuO_2 loading from 4.3 to 68.9 wt % results in a larger encircled CV area and thus higher capacitance. The encircled CV area of NMC-1-w70 is apparently larger than that of NMC-1-w30 at 20 mV/s; however, it is pretty close at 200 mV/s, suggesting a heavy loading is no longer an advantage in capacitance comparing to intermediate moderate loading when high power performance is required. At 0.2 A/g, the specific capacitances of NMC-1-w10, NMC-1-w30 and NMC-1-w70 reach 309, 401, and 430 F/g, respectively, and slightly decrease to 231, 311, and 342 F/g, respectively, at 16 A/g, as shown in Figure 7b. Moreover, the quasi-rectangular CV shape at 200 mV/s (Figure 7a) and the quasi-linear symmetric GCD curves (Figure S5b, Supporting Information) indicate capacitive behaviors in the NMC-1-wy. Also, the slow capacitance decay from 0.2 to 16 A/g in Figure 7b suggests excellent ion diffusion kinetics.

To further unveil the intrinsic properties of well-dispersed RuO_2 brought by nitrogen doping or RuO_2 phase evolution caused by RuO_2 loading, the capacitance per RuO_2 in the composite has been calculated according to eq 2:

dx.doi.org/10.1021/am502173x | ACS Appl. Mater. Interfaces 2014, 6, 9751−9759

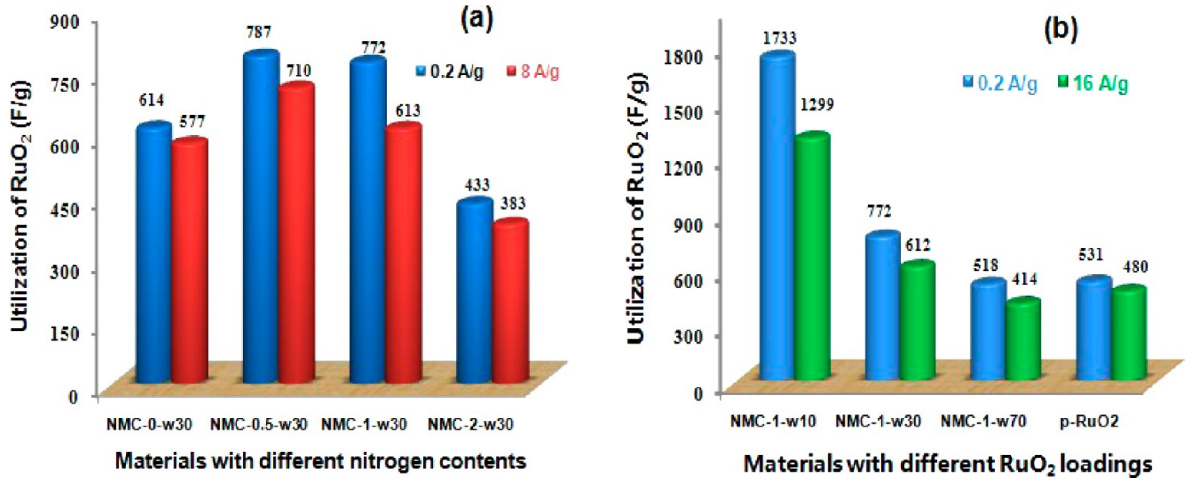

Figure 8. Utilization of RuO_2 in (a) NMC-*x*-w30 and (b) NMC-1-wy.

$$C_{s,RuO_2} = \frac{C_{s,composite} - w_{NMC} \times C_{s,NMC}}{w_{RuO_2}} \quad (2)$$

where $C_{s,NMC}$ and C_{s,RuO_2} are the specific capacitances of the NMC and RuO_2 components, respectively, while w_{NMC} and w_{RuO_2} are the weight ratios of the NMC and RuO_2 components, respectively (see Table 1). The results are presented in Figure 8. After doping 4.3 wt % N, the capacitance of RuO_2 rises from 614 F/g in NMC-0-w30 to 787 F/g in NMC-0.5-w30 at 0.2 A/g. This can be attributed to the improved RuO_2 dispersion and the enhanced electrical conductivity of the carbon framework. NMC-1-w30 with 8.1 wt % N exhibits a similar RuO_2 capacitance as NMC-0.5-w30, as their particle dispersion state and electrical conductivity are both similar. Further increasing of the nitrogen content to 11.9 wt % would harm the graphitic integrity of the structure,[28] which results in a dramatic decrease in the RuO_2 utilization to 433 F/g at 0.2 A/g.

Similarly, Figure 8b compares the capacitance of the RuO_2 component in NMC-1-wy at different current densities. Impressively, the capacitance of RuO_2 in NMC-1-w10 reaches 1733 F/g at 0.2 A/g and still maintains 1299 F/g at 16 A/g. Such a remarkable capacitance is attributed to the small amount of $RuO_2 \cdot 1.25H_2O$ (4.3 wt %) uniformly distributed within the carbon framework. Increasing RuO_2 content would reduce their utilization. At a RuO_2 loading of 68.9 wt %, capacitances of only 518 and 414 F/g are released at 0.2 and 16 A/g, respectively. The comparable results to the severely aggregated p-RuO_2 suggest that inner active sites in the larger crystallite are isolated from direct contact with protons and electrons and greatly lower the capacitance.

4. CONCLUSIONS

The presence of nitrogen species in hierarchical MCs provides additional pseudocapacitance and serves as guiding agents for the homogeneous deposition of RuO_2 NPs. It is proposed that moderate nitrogen doping (8.1 wt % N) could greatly improve the RuO_2 dispersion and enhance the capacitance per electrode, as well as per RuO_2, reaching 402 and 772 F/g at 0.2 A/g, respectively. Moreover, the electrical conductivity of the carbon backbone and the ion diffusion kinetics also benefit from moderate nitrogen doping, leading to impressively high rate performance. On the other hand, nitrogen-free or excess nitrogen worsens the electrical conductivity of the carbon, leading to RuO_2 cluster formation and a decrease in RuO_2 utilization. In addition, RuO_2 loading is also found to be an important factor in influencing both RuO_2 crystallinity and utilization. Depositing 4.3 wt % $RuO_2 \cdot 1.25H_2O$ led to a maximum capacitance of 1733 F/g per RuO_2 at 0.2 A/g. We therefore expect that other metal oxides with desirable capacitive behaviors can be incorporated into nitrogen-doped MC frameworks for high-performance supercapacitor electrodes.

■ ASSOCIATED CONTENT

Supporting Information

EDX, TGA, XRD, CV, GCD, and EIS analysis of NMC-x, NMC-1-wy, and NMC-x-w30. This material is available free of charge via the Internet at http://pubs.acs.org.

■ AUTHOR INFORMATION

Corresponding Authors

*(D.L.) E-mail: longdh@ecust.edu.cn.
*(W.Q.) E-mail: qiaowm@ecust.edu.cn.

Notes

The authors declare no competing financial interest.

■ ACKNOWLEDGMENTS

This work was partially supported by MOST (2014CB239702) and National Science Foundation of China (nos. 51302083 and 51272077), and Program of Shanghai Subject Chief Scientist (B type, no. 13XD1424900). Electron microscopy was carried out at the Drexel Centralized Research Facilities (CRF). Professor Yury Gogotsi (Drexel University) is greatly acknowledged for helpful data discussion. K. Jost is thanked for manuscript revision. L. Kong is thanked for EDX.

■ REFERENCES

(1) Simon, P.; Gogotsi, Y. Materials for Electrochemical Capacitors. *Nat. Mater.* **2008**, *7*, 845−854.
(2) Frackowiak, E.; Béguin, F. Carbon Materials for the Electrochemical Storage of Energy in Capacitors. *Carbon* **2001**, *39*, 937−950.
(3) Deng, W.; Ji, X.; Chen, Q.; Banks, C. E. Electrochemical Capacitors Utilising Transition Metal Oxides: An Update of Recent Developments. *RSC Adv.* **2011**, *1*, 1171−1178.
(4) Conway, B. *Electrochemical Supercapacitors: Scientific Fundamentals and Technological Applications*; Kluwer Academic/Plenum: New York, 1999.

(5) Xia, H.; Shirley Meng, Y.; Yuan, G.; Cui, C.; Lu, L. A Symmetric RuO_2/RuO_2 Supercapacitor Operating at 1.6 V by Using a Neutral Aqueous Electrolyte. *Electrochem. Solid-State Lett.* **2012**, *15*, A60−A63.
(6) Lin, Y.-S.; Lee, K.-Y.; Chen, K.-Y.; Huang, Y.-S. Superior Capacitive Characteristics of RuO_2 Nanorods Grown on Carbon Nanotubes. *Appl. Surf. Sci.* **2009**, *256*, 1042−1045.
(7) Lin, K.-M.; Chang, K.-H.; Hu, C.-C.; Li, Y.-Y. Mesoporous RuO_2 for the Next Generation Supercapacitors with an Ultrahigh Power Density. *Electrochim. Acta* **2009**, *54*, 4574−4581.
(8) Zhang, J.; Chu, W.; Jiang, J.; Zhao, X. S. Synthesis, Characterization and Capacitive Performance of Hydrous Manganese Dioxide Nanostructures. *Nanotechnology* **2011**, *22*, 1−9.
(9) Naguib, M.; Come, J.; Dyatkin, B.; Presser, V.; Taberna, P.-L.; Simon, P.; Barsoum, M. W.; Gogotsi, Y. MXene: A Promising Transition Metal Carbide Anode for Lithium-Ion Batteries. *Electrochem. Commun.* **2012**, *16*, 61−64.
(10) Wei, T.-Y.; Chen, C.-H.; Chang, K.-H.; Lu, S.-Y.; Hu, C.-C. Cobalt Oxide Aerogels of Ideal Supercapacitive Properties Prepared with an Epoxide Synthetic Route. *Chem. Mater.* **2009**, *21*, 3228−3233.
(11) Wang, G.; Zhang, L.; Zhang, J. A Review Of Electrode Materials for Electrochemical Supercapacitors. *Chem. Soc. Rev.* **2012**, *41*, 797−828.
(12) Lukatskaya, M. R.; Mashtalir, O.; Ren, C. E.; Dall'Agnese, Y.; Rozier, P.; Taberna, P. L.; Naguib, M.; Simon, P.; Barsoum, M. W.; Gogotsi, Y. Cation Intercalation and High Volumetric Capacitance of Two-Dimensional Titanium Carbide. *Science* **2013**, *341*, 1502−1505.
(13) Park, J. H.; Ko, J. M.; Ok Park, O. Carbon Nanotube/RuO_2 Nanocomposite Electrodes for Supercapacitors. *J. Electrochem. Soc.* **2003**, *150*, A864−A867.
(14) Lee, J.-K.; Pathan, H. M.; Jung, K.-D.; Joo, O.-S. Electrochemical Capacitance of Nanocomposite Films Formed by Loading Carbon Nanotubes with Ruthenium Oxide. *J. Power Sources* **2006**, *159*, 1527−1531.
(15) Qin, X.; Durbach, S.; Wu, G. T. Electrochemical Characterization on $Ruo_2{\cdot}xH_2O$/Carbon Nanotubes Composite Electrodes for High Energy Density Supercapacitors. *Carbon* **2004**, *42*, 451−453.
(16) Yuan, C.; Chen, L.; Gao, B.; Su, L.; Zhang, X. Synthesis and Utilization of $RuO_2{\cdot}xH_2O$ Nanodots Well Dispersed on Poly(Sodium 4-Styrene Sulfonate) Functionalized Multi-Walled Carbon Nanotubes for Supercapacitors. *J. Mater. Chem.* **2009**, *19*, 246−252.
(17) Vellacheri, R.; Pillai, V. K.; Kurungot, S. Hydrous RuO_2-Carbon Nanofiber Electrodes with High Mass and Electrode-Specific Capacitance for Efficient Energy Storage. *Nanoscale* **2012**, *4*, 890−896.
(18) Pico, F.; Ibañez, J.; Lillo-Rodenas, M. A.; Linares-Solano, A.; Rojas, R. M.; Amarilla, J. M.; Rojo, J. M. Understanding $RuO_2{\cdot}xH_2O$/Carbon Nanofibre Composites as Supercapacitor Electrodes. *J. Power Sources* **2008**, *176*, 417−425.
(19) Rakhi, R. B.; Chen, W.; Cha, D.; Alshareef, H. N. High Performance Supercapacitors Using Metal Oxide Anchored Graphene Nanosheet Electrodes. *J. Mater. Chem.* **2011**, *21*, 16197−16204.
(20) Zhang, C.; Zhou, H.; Yu, X.; Shan, D.; Ye, T.; Huang, Z.; Kuang, Y. Synthesis of RuO_2 Decorated Quasi Graphene Nanosheets and Their Application in Supercapacitors. *RSC Adv.* **2014**, *4*, 11197−11205.
(21) Zhao, Y.; Liu, L.; Xu, J.; Yang, J.; Yan, M.; Jiang, Z. High-Performance Supercapacitors of Hydrous Ruthenium Oxide/Mesoporous Carbon Composites. *J. Solid State Electrochem.* **2006**, *11*, 283−290.
(22) Zhou, Z.; Zhu, Y.; Wu, Z.; Lu, F.; Jing, M.; Ji, X. Amorphous RuO_2 Coated on Carbon Spheres as Excellent Electrode Materials for Supercapacitors. *RSC Adv.* **2014**, *4*, 6927−6932.
(23) Zhu, Y.; Ji, X.; Pan, C.; Sun, Q.; Song, W.; Fang, L.; Chen, Q.; Banks, C. E. A Carbon Quantum Dot Decorated RuO_2 Network: Outstanding Supercapacitances under Ultrafast Charge and Discharge. *Energy Environ. Sci.* **2013**, *6*, 3665−3675.
(24) Fuertes, A. B.; Lota, G.; Centeno, T. A.; Frackowiak, E. Templated Mesoporous Carbons for Supercapacitor Application. *Electrochim. Acta* **2005**, *50*, 2799−2805.
(25) Cormier, Z. R.; Andreas, H. A.; Zhang, P. Temperature-Dependent Structure and Electrochemical Behavior of RuO_2/Carbon Nanocomposites. *J. Phys. Chem. C* **2011**, *115*, 19117−19128.
(26) Jang, J. H.; Han, S.; Hyeon, T.; Oh, S. M. Electrochemical Capacitor Performance of Hydrous Ruthenium Oxide/Mesoporous Carbon Composite Electrodes. *J. Power Sources* **2003**, *123*, 79−85.
(27) Li, H.; Wang, R.; Cao, R. Physical and Electrochemical Characterization of Hydrous Ruthenium Oxide/Ordered Mesoporous Carbon Composites as Supercapacitor. *Microporous Mesoporous Mater.* **2008**, *111*, 32−38.
(28) Chen, H.; Sun, F.; Wang, J.; Li, W.; Qiao, W.; Ling, L.; Long, D. Nitrogen Doping Effects on the Physical and Chemical Properties of Mesoporous Carbons. *J. Phys. Chem. C* **2013**, *117*, 8318−8328.
(29) Hulicova-Jurcakova, D.; Seredych, M.; Lu, G. Q.; Bandosz, T. J. Combined Effect of Nitrogen- and Oxygen-Containing Functional Groups of Microporous Activated Carbon on Its Electrochemical Performance in Supercapacitors. *Adv. Funct. Mater.* **2009**, *19*, 438−447.
(30) Lota, G.; Lota, K.; Frackowiak, E. Nanotubes Based Composites Rich in Nitrogen for Supercapacitor Application. *Electrochem. Commun.* **2007**, *9*, 1828−1832.
(31) Sun, C.-L.; Chen, L.-C.; Su, M.-C.; Hong, L.-S.; Chyan, O.; Hsu, C.-Y.; Chen, K.-H.; Chang, T.-F.; Chang, L. Ultrafine Platinum Nanoparticles Uniformly Dispersed on Arrayed CN_xNanotubes with High Electrochemical Activity. *Chem. Mater.* **2005**, *17*, 3749−3753.
(32) Chen, Z.; Yu, A.; Ahmed, R.; Wang, H.; Li, H.; Chen, Z. Manganese Dioxide Nanotube and Nitrogen-Doped Carbon Nanotube Based Composite Bifunctional Catalyst for Rechargeable Zinc-Air Battery. *Electrochim. Acta* **2012**, *69*, 295−300.
(33) Fang, W.-C.; Leu, M.-S.; Chen, K.-H.; Chen, L.-C. Ultrafast Charging-Discharging Capacitive Property of RuO_2 Nanoparticles on Carbon Nanotubes Using Nitrogen Incorporation. *J. Electrochem. Soc.* **2008**, *155*, K15−K18.
(34) Zheng, J. P.; Cygan, P. J.; Jow, T. R. Hydrous Ruthenium Oxide as an Electrode Material for Electrochemical Capacitors. *J. Electrochem. Soc.* **1995**, *142*, 2699−2703.